PAPER

# A Robust and Fast Imaging Algorithm with an Envelope of Circles for UWB Pulse Radars

**Shouhei KIDERA**[†a)], ***Student Member***, **Takuya SAKAMOTO**[†], ***Member***, ***and*** **Toru SATO**[†], ***Fellow***

**SUMMARY** Target shape estimation with UWB pulse radars is a promising imaging technique for household robots. We have already proposed a fast imaging algorithm, SEABED, that is based on a reversible transform BST (Boundary Scattering Transform) between the received signals and the target shape. However, the target image obtained by SEABED deteriorates in a noisy environment because it utilizes a derivative of received data. In this paper, we propose a robust imaging method with an envelope of circles. We clarify by numerical simulation that the proposed method can realize a level of robust and fast imaging that cannot be achieved by the original SEABED.

***key words:*** *UWB pulse radars, SEABED, robust and fast imaging, high resolution imaging, envelope of circles*

## 1. Introduction

UWB pulse radar systems have great potential for a high-resolution imaging that is suitable and efficient for the measuring techniques used for household and rescue robots. Additionally, they can estimate object shapes even in the case of a fire where optical methods cannot be applied. While many imaging algorithms for radar systems have been proposed, they require intensive computation, which is not suitable for realtime operations [1]–[4]. Contrarily, we have already proposed a fast imaging algorithm called SEABED (Shape Estimation Algorithm based on BST and Extraction of Directly scattered waves) for UWB pulse radars based on a reversible transform BST between the received signals and the target shape [5], [6]. However, the image obtained by SEABED deteriorates in a noisy environment because it utilizes derivatives of the received data. To resolve this problem, image stabilization methods have been proposed. One of these utilizes an adaptive smoothing with Gaussian filter [7], another is based on Fractional Boundary Scattering Transform [8]. These two methods are robust in a noisy environment. However, they both still utilize the BST with derivatives of received data and so cannot completely remove the instability.

To resolve this problem, in this paper we propose a robust imaging algorithm with an envelope of circles, which does not sacrifice the speed of SEABED. We note that a conventional method quoted in [9] is similar to our approach from the viewpoint that it extracts the target boundary with time delays. Additionally, this method achieves robust imaging in a noisy environment because it does not utilize a derivative operation. However, this method can be applied only to convex targets. In this paper, we propose a fast and robust imaging algorithm for arbitrary shaped targets. We calculate circles with estimated delays for each antenna location and utilize the principle that these circles circumscribe or inscribe the target boundary. With this principle, we prove that the target boundary is expressed as a boundary of a union and an intersection set of the circles. This method does not utilize a derivative of received data, and enables us to realize robust imaging for an arbitrary shape target.

Manuscript received September 4, 2006.
Manuscript revised January 26, 2007.

[†]The authors are with the Department of Communications and Computer Engineering, Graduate School of Informatics, Kyoto University, Kyoto-shi, 606-8501 Japan.
a) E-mail: kidera@aso.cce.i.kyoto-u.ac.jp

DOI: 10.1093/ietcom/e90–b.7.1801

## 2. System Model

We deal with 2-dimensional problems and TE mode waves. We assume that the target has uniform permittivity and is surrounded by a clear boundary that is composed of smooth curves concatenated at discrete edges. We also assume that the propagation speed of the radiowave is constant and known. We assume a mono-static radar system. The induced current at the transmitting antenna is a mono-cycle pulse.

We define r-space as the real space where targets and antennae are located. We express r-space with the parameters $(x, y)$. An omni-directional antenna is scanned along the $x$ axis. Both $x$ and $y$ are normalized by $\lambda$, which is the center wavelength of the transmitted pulse. We assume $y > 0$ for simplicity. We define $s'(X, Y)$ as the received electric field at the antenna location $(x, y) = (X, 0)$, where we define $Y$ with the arrival time of the echo $t$ and the speed of the radio wave c as $Y = ct/(2\lambda)$. We apply a matched filter with the transmitted waveform to $s'(X, Y)$. We define $s(X, Y)$ as the output of the filter. We define d-space as the space expressed by $(X, Y)$, and call it a quasi wavefront.

## 3. Conventional Method

### 3.1 SEABED Algorithm

We have already developed a non-parametric shape estimation algorithm called SEABED. This method utilizes a reversible transform BST between the point of r-space $(x, y)$ and the point of d-space $(X, Y)$, which is extracted by the output of the matched filter $s(X, Y)$. BST is expressed as

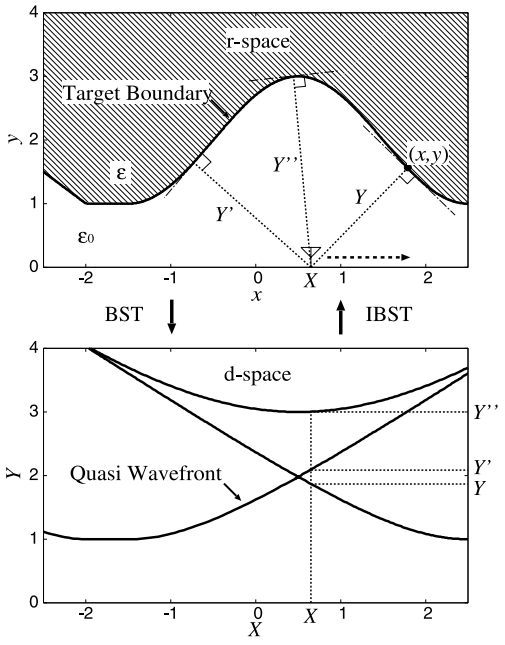


**Fig. 1** Relationship between r-space (Upper side) and d-space (Lower side).

$$\left.\begin{aligned} X &= x + y\mathrm{d}y/\mathrm{d}x. \\ Y &= y\sqrt{1 + (\mathrm{d}y/\mathrm{d}x)^2}. \end{aligned}\right\} \tag{1}$$

IBST (Inverse BST) is expressed as

$$\left.\begin{aligned} x &= X - Y\mathrm{d}Y/\mathrm{d}X. \\ y &= Y\sqrt{1 - (\mathrm{d}Y/\mathrm{d}X)^2}, \end{aligned}\right\} \tag{2}$$

where $|\mathrm{d}Y/\mathrm{d}X| \leq 1$ holds. This transform is reversible, and gives us a complete solution for the inverse problem. Figure 1 shows the relationship between the r-space and the d-space. IBST utilizes the characteristic that an incident wave is intensively reflected in the normal direction. By utilizing IBST, SEABED enables us to estimate the target boundary directly from a quasi wavefront. SEABED has the advantage that it can directly estimate target boundaries with IBST, and achieves fast, high resolution imaging.

### 3.2 Noise Tolerance of SEABED

In a noisy environment, the estimated image with SEABED easily deteriorates because IBST utilizes the derivative of a quasi wavefront. In this section, we examine the behavior of SEABED in a noisy environment. We scan an antenna in $-2.5\lambda \leq x \leq 2.5\lambda$, and receive data at 101 locations. We give a quasi wavefront with random error whose standard deviation is $0.005\lambda$. We smooth the quasi wavefront with Gaussian filter. Figures 2, 3 and 4 show the estimated boundary by applying IBST to the quasi wavefront where we set the correlation length of the filter as $0.05\lambda$, $0.2\lambda$ and $0.1\lambda$, respectively. In Fig. 2, the estimated points have large errors around the edge. This is because the correlation length is too short. To discuss the deterioration of the image analytically, we rewrite IBST as

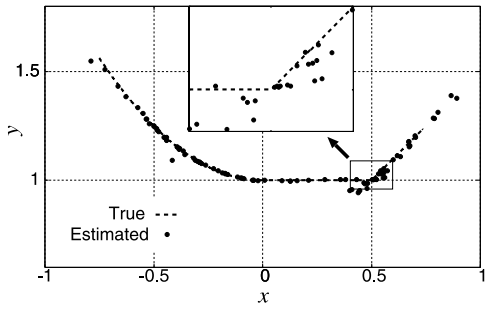


**Fig. 2** An estimated image with SEABED where correlation length is set to $0.05\lambda$.

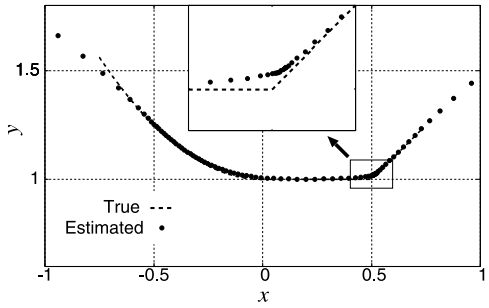


**Fig. 3** Same as Fig. 2 but correlation length is set to $0.2\lambda$.

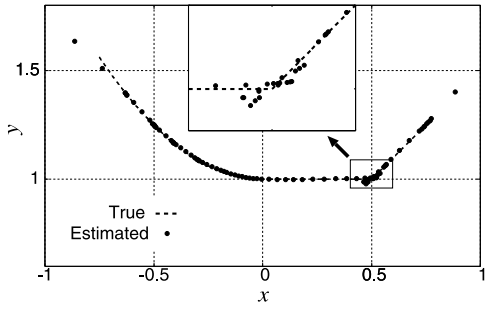


**Fig. 4** Same as Fig. 2 but correlation length is set to $0.1\lambda$.

$$\left.\begin{aligned} x &= X + Y\cos\theta \\ y &= Y\sin\theta \end{aligned}\right\}, \tag{3}$$
$$\theta = \cos^{-1}(-\mathrm{d}Y/\mathrm{d}X), \quad (0 \leq \theta < \pi),$$

where $\theta$ is expressed as in Fig. 1. Equation (3) means that the estimated points with IBST are on the circle whose center is $(X, 0)$ and radius is $Y$. In the equation, $\theta$ is determined with $\mathrm{d}Y/\mathrm{d}X$. Therefore, the estimated point mistakenly plots along this circle in a noisy environment because the accuracy of $\theta$ strongly depends on that of $\mathrm{d}Y/\mathrm{d}X$.

While the estimated image in Fig. 3 is stable, the resolution of the image degrades, especially around the edge. Accordingly, SEABED suffers from a trade-off between the stability and the resolution of the estimated image. Therefore, we empirically choose the correlation length as $0.1\lambda$ which holds the resolution and a stability of the image as shown in Fig. 4. However the estimated points in Fig. 4 still have errors.

To resolve this trade-off with SEABED, methods for stabilizing images have been proposed. One method is based on smoothing the quasi wavefront, where we change the standard deviation of the Gaussian filter depending on the target shape [7]. Another is based on smoothing the data obtained in the intermediate space between the r-space and the d-space using Fractional Boundary Scattering Transform [8]. These methods achieve robust imaging in a noisy environment. However, they cannot completely resolve the above trade-off because they still depend on the derivative operations.

## 4. Proposed Method

### 4.1 A Target Boundary and Envelopes of Circles

To resolve the trade-off between the stability and resolution of SEABED as set out in the previous section, we propose a new imaging algorithm that is free from derivative operations. First, we clarify the relationship between the group of points on a target boundary and that on the envelope of the circles. We assume that the target boundary $\partial T$ is expressed as a single-valued and differentiable function. $(X, Y)$ is a point on $\partial D$, which is the quasi wavefront of $\partial T$. We define $\Gamma$ as the domain of $X$ for $\partial D$. We define $g(X, Y) = \partial x/\partial X = 1 - (\mathrm{d}Y/\mathrm{d}X)^2 - Y\mathrm{d}^2Y/\mathrm{d}X^2$, and $\gamma$ as the domain of $x$ for $\partial T$. We define $S_{(X,Y)}$ as an open set, which is defined as an interior of the circle which satisfies $(x - X)^2 + y^2 = Y^2$. Figures 5 and 6 show the relationship between d-space and r-space for a convex and a concave targets, respectively. If $\partial D$ is a single-valued and continuous function, we define $S_+ = \bigcup_{X\in\Gamma} S_{(X,Y)}$ and $S_\times = \bigcap_{X\in\Gamma} S_{(X,Y)}$. We define the boundary $\partial S_+$ as

$$\partial S_+ = \{(x, y) \mid (x, y) \in \overline{S_+} - S_+,\ x \in \gamma,\ y > 0\}, \tag{4}$$

and $\partial S_\times$ as

$$\partial S_\times = \{(x, y) \mid (x, y) \in \overline{S_\times} - S_\times,\ x \in \gamma,\ y > 0\}, \tag{5}$$

where $\overline{S_+}$ and $\overline{S_\times}$ is a closure of $S_+$ and $S_\times$, respectively.

Here the next equation holds

$$\partial T = \begin{cases} \partial S_+ & (g(X, Y) > 0), \\ \partial S_\times & (g(X, Y) < 0). \end{cases} \tag{6}$$

The proof of Eq. (6) is given in Appendix A. Eq. (6) shows that $\partial S_+$ and $\partial S_\times$ express the target boundary as an envelope of circles depending on the sign of $g(X, Y)$ as shown in Figs. 5 and 6. We should correctly select these methods considering the sign of $g(X, Y)$. We utilize the next proposition.

**Proposition 1:** The necessary and sufficient condition of $g(X, Y) < 0$ is that

$$\overline{S_+} \subset \overline{S_{\max} \cup S_{\min}} \tag{7}$$

Here, we define $(X_{\max}, Y_{\max})$ and $(X_{\min}, Y_{\min})$ as the point of $\partial D$, where $X_{\max}$ and $X_{\min}$ are the maximum and minimum values, respectively, at $X \in \Gamma$, as shown in Fig. 6. We define $S_{\max}$ and $S_{\min}$ express $S_{(X_{\max},Y_{\max})}$ and $S_{(X_{\min},Y_{\min})}$, respectively. A proof of Proposition 1 is given in Appendix B.

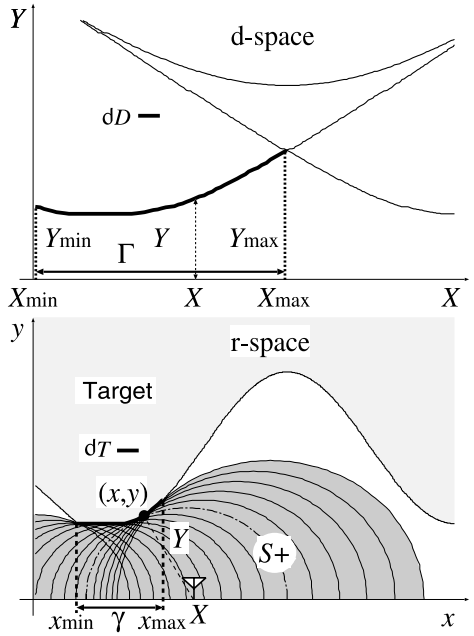


**Fig. 5** Quasi wavefront (Upper side) and a convex target boundary and an envelope of circles (Lower side).

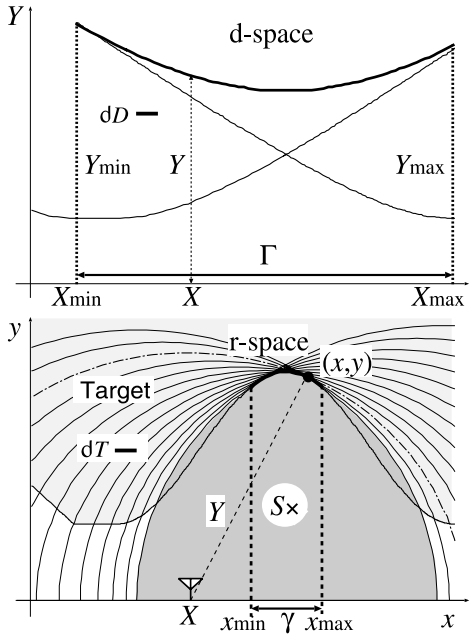


**Fig. 6** Quasi wavefront (Upper side) and a concave target boundary and an envelope of circles (Lower side).

If $g(X, Y) < 0$ holds, all circles for $X \in \Gamma$ should inscribe to the target boundary. This condition corresponds to that $x(X_{\max}, X) < x(X_{\max}, X_{\min}) < x(X_{\min}, X)$ holds for all $X \in \Gamma$ as shown in Fig. A· 3, where $x(X, X')$ is $x$ coordinates of the intersection point of $\partial S_{(X,Y)}$ and $\partial S_{(X',Y')}$. This condition is

equivalent to Eq. (7) that all $S_{(X,Y)}$ in $X \in \Gamma$ are included in $S_{\max}$ and $S_{\min}$. Accordingly, the number of circles which constitute $\overline{S_+}$ should be 2 in minimum for $g(X,Y) < 0$. We should search the minimum number of the circles which constitute $\overline{S_+}$. If the minimum number is 2, $\partial T = \partial S_\times$ holds; otherwise, $\partial T = \partial S_+$ holds. When a target boundary includes an edge, the edge can be estimated as the intersection point of circles $\partial S_{(X,Y)}$, where $(X,Y)$ is transformed into the edge point $(x,y)$ with the IBST. Therefore, the target boundary $\partial T$ with edges can be expressed as one of $\partial S_+$ and $\partial S_\times$.

In our proposed method, we estimate the target boundary with an envelope of circles by utilizing these relationships. This method enables us to transform the group of points $(X,Y)$ to the group of points $(x,y)$ without a derivative operation. Note that we receive the scattered wave that passes through a caustic point if the quasi wavefronts satisfies $g(X,Y) < 0$. In that case, a phase of the scattered waveform rotates by $\pi/2$ [6]. We can robustly recognize this phase rotation from $(X,Y)$ with the sufficient condition of proposition 1. We compensate this phase rotation in our proposed method to enhance the accuracy of the estimated image.

### 4.2 Procedures in the Proposed Method

The actual procedures of the proposed method are as follows. Here we define $R(X,X')$ as $x$ coordinates of the intersection point of $\partial S_{(X,Y)}$ and $\partial S_{(X',Y')}$. We also define $\Delta X$ as the sampling interval of the antenna.

Step 1). Apply the matched filter to the received signals $s'(X,Y)$ and obtain the output $s(X,Y)$.

Step 2). Extract quasi wavefronts as $(X,Y')$ which satisfies $\partial s(X,Y)/\partial Y = 0$, $|s(X,Y)| \geq \alpha \cdot \max_Y |s(X,Y)|$. Extract $(X,Y)$ as $\partial D_{\mathrm{T}}$ from $(X,Y')$, which satisfies the local maximum of $Y'$ for each $X$. Parameter $\alpha$ and the searching region of $Y'$ are determined empirically.

Step 3). Extract a set of $(X,Y)$ as $\partial D_i$ from $\partial D_{\mathrm{T}}$, which is continuous and $|\mathrm{d}Y/\mathrm{d}X| \leq 1$ is satisfied.

Step 4). Extract boundary points $(x,y)$ on $\partial S_+$ $(X,Y) \in \partial D_i$ as

$$y = \max_{X \in \Gamma_i} \sqrt{Y^2 - (x-X)^2}, \tag{8}$$

where $\Gamma_i$ is a domain of $X$ where $(X,Y) \in \partial D_i$ satisfies. Count the minimum number of circles which constitute $S_+$, and define the number as $N_{\mathrm{C}}$. If $N_{\mathrm{C}} > 2$, determine

$$\partial T_i = \partial S_+, \ (x_{\min} \leq x \leq x_{\max}), \tag{9}$$

where $x_{\min} = R(X_{\min}, X_{\min} + \Delta X)$ and $x_{\max} = R(X_{\max}, X_{\max} - \Delta X)$.

If $N_{\mathrm{C}} = 2$, compensate a phase rotation for $s(X,Y)$ by $\pi/2$ and renew the quasi wavefronts as $(X,Y_{\mathrm{c}})$, and extract boundary points $(x,y)$ on $\partial S_\times$ as

$$y = \min_{X \in \Gamma_i} \sqrt{Y_{\mathrm{c}}^2 - (x-X)^2}. \tag{10}$$

Determine

$$\partial T_i = \partial S_\times, \ (x_{\min} \leq x \leq x_{\max}), \tag{11}$$

where $x_{\min} = R(X_{\max}, X_{\max} - \Delta X)$ and $x_{\max} = R(X_{\min}, X_{\min} + \Delta X)$.

Step 5). Set $i = i + 1$, and iterate Step 3) and 4) until $\partial D_{\mathrm{T}}$ becomes empty.

Step 6). Estimate the target boundary as $\partial T = \bigcup_i \partial T_i$.

## 5. Performance Evaluation

### 5.1 Shape Estimation Examples

We evaluate the estimation accuracies of SEABED and the method we propose here. First, we give the random errors to the true quasi wavefront, which is calculated from the true target boundary with BST. The standard deviation of the noise is $0.005\lambda$. This simulation estimates the accuracy without influences from other factors including waveform distortion. The signals are received at 101 locations for $-2.5\lambda \leq x \leq 2.5\lambda$. We fix the correlation length to $0.1\lambda$ from the results of 3.2. Figure 7 shows the estimated image where we apply the proposed method to the same data as Fig. 2. The estimated image with the proposed method achieves more stable and high-resolution imaging than SEABED, especially around the edge. Figures 8 and 9 show the estimated images of the concave target achieved with SEABED and the proposed method, respectively. The estimated image for the concave shape with SEABED is not stable, especially at around $x = 0, \pm 2$. Contrarily, the estimated image with the proposed method is more stable and accurate. This is because the proposed method estimates the inclination of the target as that of the circles, which circumscribe or inscribe to the target boundary. A part of the circles contributes as a part of the estimated shape, which means

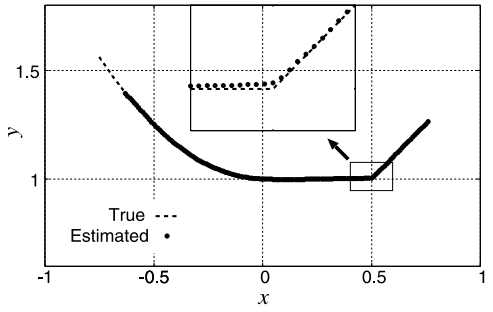


**Fig. 7** Estimated image with the proposed method for a convex target with noise.

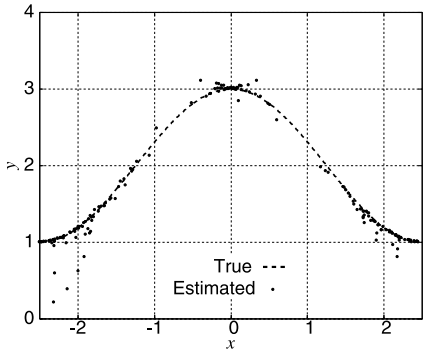


**Fig. 8** Estimated image with SEABED for a concave target with noise.

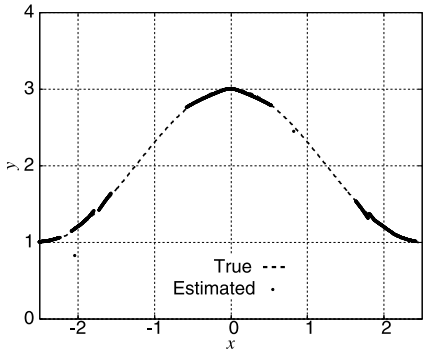


**Fig. 9** Estimated image with the proposed method for a concave target with noise.

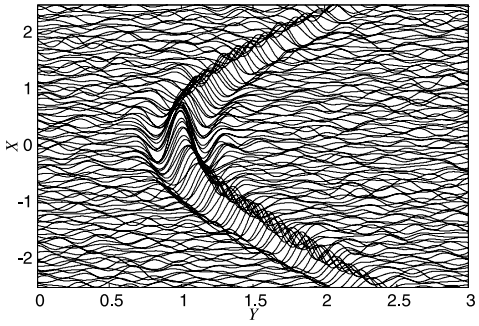


**Fig. 10** Output of the matched filter for a convex target.

that the inclination of the circle is utilized for imaging.

Next, we add a white noise to the received data $s'(X, Y)$ calculated with the FDTD method. Figure 10 shows the output of the matched filter with the transmitted waveform. In this case, S/N is about 5.5 dB. Here we define S/N as

$$\mathrm{S/N} = \frac{1}{\sigma_{\mathrm{N}}^2 (X_{\max} - X_{\min})} \int_{X_{\min}}^{X_{\max}} \max_{Y} |s(X, Y)|^2 \mathrm{d}X, \qquad (12)$$

where $X_{\max}$ and $X_{\min}$ are the maximum and minimum antenna locations, respectively, and $\sigma_{\mathrm{N}}$ is the standard deviation of noise. Figures 11 and 12 show the estimated images with SEABED and the proposed method, respectively. The image of SEABED is not accurate especially around the edges of the target. Contrarily, the image obtained by the proposed method is stable, although the image around the

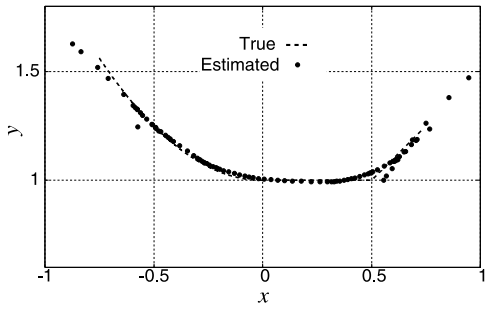


**Fig. 11** Estimated image with SEABED for a convex target with noise to $s'(X, Y)$.

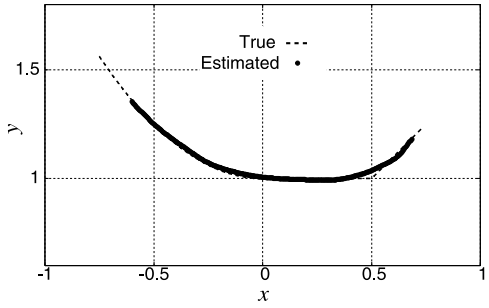


**Fig. 12** Estimated image with the proposed method for a convex target with noise to $s'(X, Y)$.

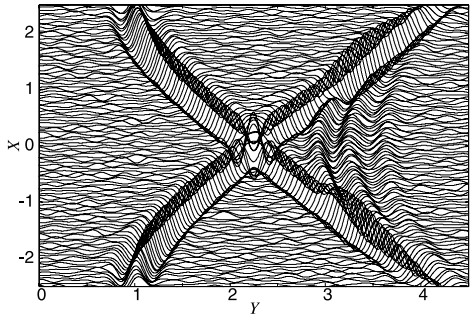


**Fig. 13** Output of the matched filter for a concave target.

edge is not precise compared with Fig. 7. We confirm that the same image distortion around the edge appear in a noiseless case. Therefore, the image distortion is caused by the edge diffraction waveform which is different from the transmitted one. We should also estimate the scattered waveform by using the estimated image to enhance the accuracy [10]. This will be an important future work.

Next, we deal with scattered signals for a concave target. Figure 13 shows the output of the matched filter. S/N is about 8.0 dB. Figures 14 and 15 show the estimated images for a concave target with SEABED and the proposed method, respectively. The proposed method can estimate a more stable and accurate image than can be achieved with SEABED. The phase rotation of the scattering at the concave surface is correctly compensated. The calculation time of SEABED is 10.0 msec. The proposed method requires more than 10.0 msec. This is because our method requires

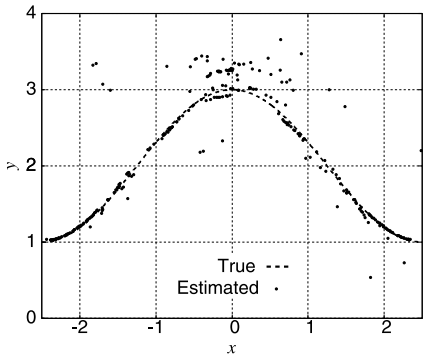


**Fig. 14** Estimated image with SEABED for a concave target with noise to $s'(X, Y)$.

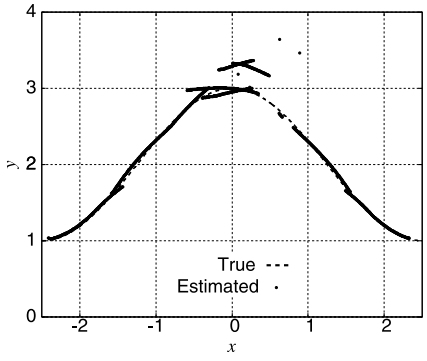


**Fig. 15** Estimated image with the proposed method for a concave target with noise to $s'(X, Y)$.

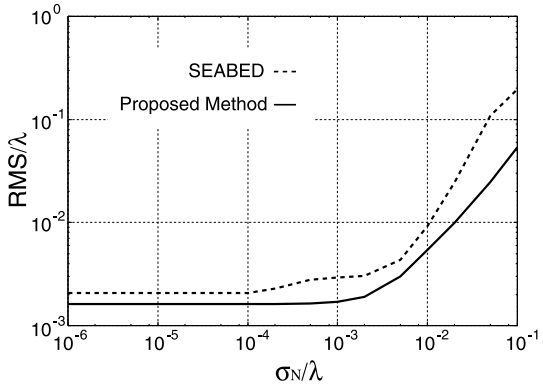


**Fig. 16** Relationship between RMS and $\sigma_N$ for a convex target.

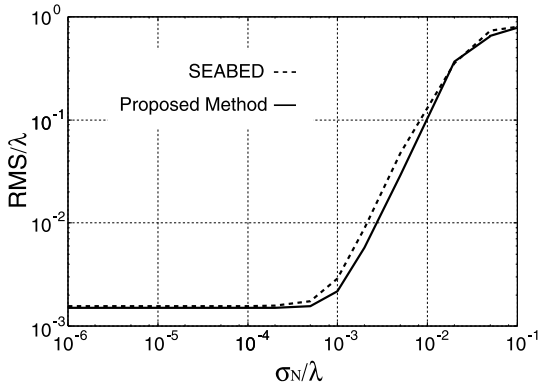


**Fig. 17** Relationship between RMS and $\sigma_N$ for a concave target.

searching operation in Eqs. (8) and (10). This computational time is short enough for real time imaging. Additionally, due to multiple scattering, false images are seen above the target boundary. To develop a robust algorithm without false images will also be a future task.

We should compare our method with the conventional method [8]. Fractional boundary scattering transform enables us to deal with the intermediate space between r-space and d-space. With this transform, we can adaptively smooth data depending on the target shapes. The optimized way of smoothing with FBST is equal to the smoothing in the d-space for the assumed target shapes in Figs. 4 and 8. Therefore, Figs. 4 and 8 correspond to the optimal smoothing method with FBST.

### 5.2 Accuracy Limitation to Noise

In this section, we quantitatively evaluate the accuracy of the estimated image with the proposed algorithm. We give random errors to the true quasi wavefront. Figures 16 and 17 show the root mean square errors (abbreviated as RMS) for the convex and the concave target, respectively. The number of trial is 500. Our method obtains 2 times improvement in accuracy for the both targets compared to SEABED, where $\sigma_N = 5.0 \times 10^{-3}$. These improvements do not depend on the noise power. Also, the accuracy of each method is larger than $1.0 \times 10^{-3}$. This is because the quasi wavefront is smoothed with the Gaussian filter whose correlation length is $0.1\lambda$, which causes a systematic error. Although RMS depends on the correlation length of the Gaussian filter, we confirm that RMS of the proposed method is better than that of SEABED regardless of the correlation length. The reasons of these results are as follows. SEABED determines a point of the target boundary with derivative operations. Contrarily, the proposed method utilizes all of the points of a quasi wavefront in Eqs. (8) and (10). Therefore, this method absorbs the instability of the derivative operations with the wider information of a quasi wavefront.

Moreover, we see the fluctuations of errors with SEABED in Fig. 16. We see the same fluctuation, even if we increase the number of the trial to 10000. The reason is that the relationship between the accuracy and the noise intensity is not simple because SEABED utilizes derivative operations. Additionally, the accuracy of each method depends on the local shape of the target. Figures 18 and 19 show the estimation error of $y$ for each $x$ in the both targets ($\sigma_N = 5.0 \times 10^{-3}\lambda$). As shown in Fig. 18, the error around the edge region becomes large even in the low noise situation. Though we assume that the antenna is scanned along the straight line in the paper, this method can be readily extended to scanning along an arbitrary curved line.

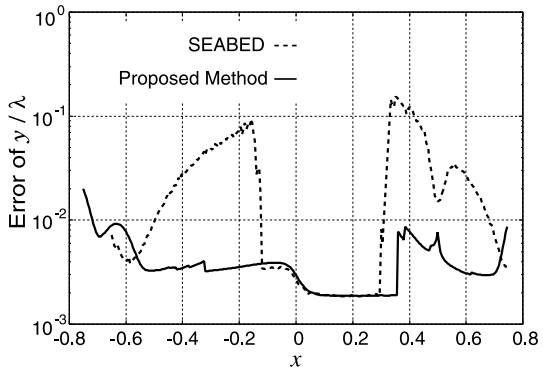


**Fig. 18** Estimation error of $y$ for each $x$ in a convex target ($\sigma_N = 5.0 \times 10^{-3}\lambda$).

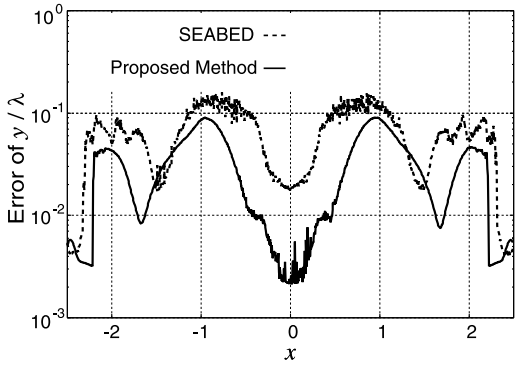


**Fig. 19** Estimation error of $y$ for each $x$ in a concave target. ($\sigma_N = 5.0 \times 10^{-3}\lambda$).

## 6. Conclusion

We proposed a stable and fast imaging method using an envelope of circles. We clarified that convex and concave target boundaries can be expressed as the boundary of the union and the intersection, respectively, of a set of circles obtained by quasi wavefronts. We clarified that the proposed method can estimate images that be more stable and accurate than those obtained with SEABED in numerical simulations. Further, the proposed method achieves fast imaging, just like with SEABED. An important future work will be to extend this algorithm to 3-dimensional problems, and to achieve a higher-resolution to compensate for the waveform distortion.

## Acknowledgment

This work is supported in part by the 21st Century COE Program (Grant No. 14213201).

### References

[1] C. Chiu, C. Li, and W. Chan, "Image reconstruction of a buried conductor by the genetic algorithm," IEICE Trans. Electron., vol.E84-C, no.12, pp.1946–1951, Dec. 2001.
[2] T. Takenaka, H. Jia, and T. Tanaka, "Microwave imaging of an anisotropic cylindrical object by a forward-backward time-stepping method," IEICE Trans. Electron., vol.E84-C, no.12, pp.1910–1916, Dec. 2001.
[3] T. Sato, K. Takeda, T. Nagamatsu, T. Wakayama, I. Kimura, and T. Shinbo, "Automatic signal processing of front monitor radar for tunneling machines," IEEE Trans. Geosci. Remote Sens., vol.35, no.2, pp.354–359, 1997.
[4] T. Sato, T. Wakayama, and K. Takemura, "An imaging algorithm of objects embedded in a lossy dispersive medium for subsurface radar data processing," IEEE Trans. Geosci. Remote Sens., vol.38, no.1, pp.296–303, 2000.
[5] T. Sakamoto and T. Sato, "A target shape estimation algorithm for pulse radar systems based on boundary scattering transform," IEICE Trans. Commun., vol.E87-B, no.5, pp.1357–1365, May 2004.
[6] T. Sakamoto and T. Sato, "A phase compensation algorithm for high-resolution pulse radar systems," IEICE Trans. Commun., vol.E87-B, no.6, pp.1631–1638, June 2004.
[7] T. Sakamoto and T. Sato, "An experimental study on a fast and accurate 3-D imaging algorithm for UWB pulse radar systems," 28th General Assembly of International Union of Radio Science (URSI), F05.7, Oct. 2005.
[8] T. Sakamoto and T. Sato, "An accurate shape estimation method with the adaptive fractional boundary scattering transform for UWB pulse radars," 34th Electromagnetic Theory Symposium, EMT–05-57, Nov. 2005.
[9] M. Tsunasaki, H. Mitsumoto, and M. Kominami, "Aperture estimation of the underground pipes by ellipse estimation from ground penetrating radar image," IEICE Technical Report, SANE2003–52, Sept. 2003.
[10] S. Kidera, T. Sakamoto, and T. Sato, "A high-resolution imaging algorithm based on scattered waveform estimation for UWB pulse radar systems," Proc. 2005 IEEE International Geoscience and Remote Sensing Symposium, pp.1725–1728, July 2005.

## Appendix A: Proof of Eq. (6)

First, let us prove that if $g(X, Y) > 0$ holds at $(X, Y) \in \partial D$, $\partial S_{(X,Y)}$ circumscribes $\partial T$, where we define $\partial S_{(X,Y)}$ as the boundary of $S_{(X,Y)}$. With $(x, y) \in \partial T$, the curvature $\kappa$ on $\partial T$ is expressed as

$$\kappa = \frac{\mathrm{d}^2 y/\mathrm{d}x^2}{(1 + (\mathrm{d}y/\mathrm{d}x)^2)^{3/2}} \quad (\mathrm{A}\cdot 1)$$

$$= \frac{\ddot{Y}}{1 - Y\ddot{Y} - \dot{Y}^2}. \quad (\mathrm{A}\cdot 2)$$

where we define $\dot{Y} = \mathrm{d}Y/\mathrm{d}X$, $\ddot{Y} = \mathrm{d}^2 Y/\mathrm{d}X^2$, and utilize $\mathrm{d}y/\mathrm{d}x = \dot{Y}/\sqrt{1 - \dot{Y}^2}$, and $\mathrm{d}^2 y/\mathrm{d}x^2 = \frac{\ddot{Y}}{(1-\dot{Y}^2)^{3/2}(1-Y\ddot{Y}-\dot{Y}^2)}$, which are derived in [6]. Here, the condition that $\partial S_{(X,Y)}$ circumscribes $\partial T$ is that $\kappa > -1/Y$ holds because a curvature of $\partial S_{(X,Y)}$ should be $-1/Y$ for $y \geq 0$. If $g(X, Y) > 0$ holds, this condition is expressed as $1 - (\mathrm{d}Y/\mathrm{d}X)^2 > 0$, which is satisfied because $y$ is a real number in the IBST. Therefore, the previous proposition is proved. Similarly, we can prove that if $g(X, Y) < 0$ holds at $(X, Y) \in \partial D$, $\partial S_{(X,Y)}$ inscribes $\partial T$. By utilizing these facts, the next proposition holds,

**Proposition 2:** If $g(X, Y) > 0$ holds at $\partial D$ and $(x, y) \in \partial T$, $x \in \gamma$ holds, $(x - X)^2 + y^2 \geq Y^2$ is satisfied for all $(X, Y) \in \partial D$, and $(X, Y)$ exists as only one, where an equal sign holds.

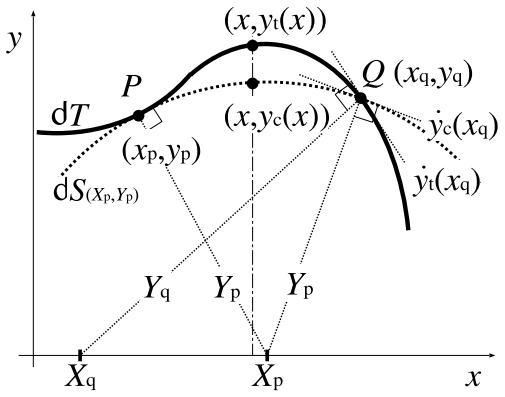


**Fig. A· 1** Arrangement of $P$, $Q$, $S_{(X_p,Y_p)}$ and $\partial T$ for the proof of Proposition 2.

We show the proof of this proposition as follows. We define $(x_p, y_p) \in \partial T, x_p \in \gamma$ as the circumscription point of $\partial S_{(X_p,Y_p)}$ where $(X_p, Y_p) \in \partial D$. We assume that $\partial S_{(X_p,Y_p)}$ exists, which intersects $\partial T$ except for $(x_p, y_p)$ as shown in Fig. A· 1. We define this intersection point as $Q = (x_q, y_q)$, where $x_q > x_p$, $x_q \in \gamma$ holds, and other intersection points do not exist for the region $x_p < x < x_q$. We also define $(X_q, Y_q)$, which is transformed from $(x_q, y_q)$ with BST. Here $(X_q, Y_q) \in \partial D$ holds because $(x_q, y_q) \in \partial T$. We define the points as $(x, y_t(x)) \in \partial T$ and $(x, y_c(x)) \in \partial S_{(X_p,Y_p)}$ for the region $x_p \le x \le x_q$. In this region, $y_t(x) \ge y_c(x)$ holds because $\partial S_{(X_p,Y_p)}$ circumscribes $\partial T$ at $P$. We also define the inclination of $\partial T$ and $\partial S_{(X_p,Y_p)}$ at $Q$ as $\dot{y}_t(x_q)$ and $\dot{y}_c(x_q)$, respectively. Here $\dot{y}_t(x_q) \le \dot{y}_c(x_q)$ holds because $y_t(x) \ge y_c(x)$ holds for $x_p \le x \le x_q$. Contrarily, $X_q > X_p$ holds because $g(X, Y) > 0$ and $x_q > x_p$ holds. Therefore, $\dot{y}_t(x_q) > \dot{y}_c(x_q)$ satisfies because $X_q = x_q + y_q\dot{y}_t(x_q)$ and $X_p = x_q + y_q\dot{y}_c(x_q)$ hold. These facts contradict each other, and $\partial S_{(X_p,Y_p)}$ circumscribes $\partial T$ at only one point at $P$. It is also proved if $x_p > x_q$ holds. Therefore, $(x - X_p)^2 + y^2 \ge Y_p^2$ holds for $(x, y) \in \partial T$. Similarly, this is satisfied for all $(X, Y) \in \partial D$. Thus, the proposition 2 is proved. Similarly, we prove that if $g(X, Y) < 0$ holds at $\partial D$ and $(x, y) \in \partial T$, $x \in \gamma$ holds, $(x - X)^2 + y^2 \le Y^2$ satisfies for all $(X, Y) \in \partial D$, and $(X, Y)$ exists as only one, where an equal sign holds.

Here we prove $\partial T = \partial S_+$ as follows.

(a) Proof of $\partial S_+ \subset \partial T$. We assume that the point $P = (x_p, y_p)$, $(x_p \in \gamma)$ exists, where $P \in \partial S_+$, $P \notin \partial T$. We define the point $Q = (x_p, y_q) \in \partial T$ as shown in Fig. A· 2. Here, $(X_p, Y_p) \in \partial D$ exists, where $(x_p - X_p)^2 + y_p^2 = Y_p^2$ holds. On the other hand, $(x_p - X_p)^2 + y_q^2 \ge Y_p^2$ holds with Prop. 2. Therefore $y_q \ge y_p$ holds because $y_q, y_p > 0$. Moreover, $y_q > y_p$ because we assume $P \notin \partial T$. Here we define $(X_q, Y_q) \in \partial D$ which is transformed from $(x_p, y_q)$ with BST. Here $(X_q - x_p)^2 + y_p^2 < Y_q^2$ holds because of $(X_q - x_p)^2 + y_q^2 = Y_q^2$ and $y_q > y_p$. Therefore $P \in S_{(X_q,Y_q)}$ holds. $P \in S_+$ holds because of $S_{(X_q,Y_q)} \subset S_+$. However $\partial S_+ \cap S_+ = \phi$ holds, where $\phi$ is null set, because $S_+$ is open set. Accordingly, $P \notin \partial S_+$ should not hold. Therefore $\partial S_+ \subset \partial T$ is proved.

(b) Proof of $\partial T \subset \partial S_+$, $(x \in \gamma)$.

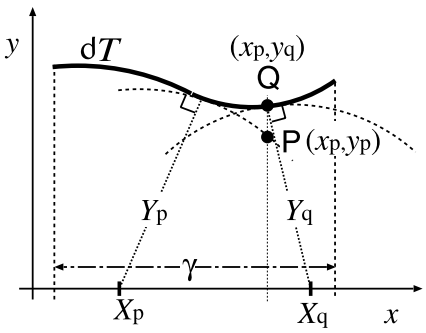


**Fig. A· 2** Arrangement of $P$, $Q$ and $\partial T$ for the proof of $\partial S_+ \subset \partial T$.

We assume that $P = (x_p, y_p)$ will exist where $P \in \partial T$, $P \notin \partial S_+$ holds. Here it is obvious with the definition of $\partial S_+$ that the sufficient condition of $(x, y) \in \partial S_+$ is that for all $(X, Y) \in \partial D$, $(x - X)^2 + y^2 \ge Y^2$ holds and $(X, Y) \in \partial D$ exists at least one point where an equal sign holds. On the contrary, $P$ satisfies the sufficient condition of $(x, y) \in \partial S_+$ with Prop. 2 because $P \in \partial T$ and $g(X, Y) > 0$ holds. Accordingly, the previous assumption is not true, and $\partial T \subset \partial S_+$ is proved.

With the facts (a),(b), $\partial T = \partial S_+$ is proved, where $g(X, Y) > 0$ holds. Similarly, we can prove that $\partial T = \partial S_\times$ where $g(X, Y) < 0$ holds.

## Appendix B: Proof of Proposition 1

(i) Proof of the necessary condition of Proposition 1.
Here $\partial T = \partial S_\times$ holds because $g(X, Y) < 0$. We define $(X_q, Y_q) \in \partial D$, where $X_q \ne X_{\max}, X_{\min}$ holds. We define the point $Q = (x_q, y_q) \in \partial T$, which is transformed from $(X_p, Y_p)$ with IBST as shown in Fig. A· 3. Here we also define $(x_{\min}, y_{\min}) \in \partial T$ which is transformed from $(X_{\min}, Y_{\min})$. Here, for all $(X, Y) \in \partial D$, $(X - x)^2 + y^2 \le Y^2$ holds at $(x, y) \in \partial T$ because $g(X, Y) < 0$ holds. Therefore, $(X_{\min} - x_q)^2 + y_q^2 < Y_{\min}^2$ and $(X_q - x_{\min})^2 + y_{\min}^2 < Y_q^2$ hold because $x_q \ne x_{\min}$ holds for $X_q \ne X_{\min}$. We define the points on $\partial S_{(X_q,Y_q)}$ and $\partial S_{\min}$ as $(x, y_Q(x))$ and $(x, y_{MIN}(x))$, respectively. Here, $y_Q(x_q)^2 < Y_{\min}^2 - (x_q - X_{\min})^2 = y_{MIN}(x_q)^2$ holds. Also, $y_{MIN}(x_{\min})^2 < Y_q^2 - (x_{\min} - X_q)^2 = y_Q(x_{\min})^2$ holds. Therefore, $y_Q(x_q) < y_{MIN}(x_q)$ and $y_Q(x_{\min}) > y_{MIN}(x_{\min})$ hold because we assume $y \ge 0$. Accordingly, $\partial S_{(X_q,Y_q)}$ and $\partial S_{\min}$ intersect at the region $x_q < x < x_{\min}$ because $x_q < x_{\min}$ for $g(X, Y) < 0$. Here the intersection point of these two circles exists as only one because we assume $y \ge 0$. Therefore, $y_Q(x) < y_{MIN}(x)$ holds for $x \le x_q$, and $\partial S_{(X_q,Y_q)} \subset \overline{S_{\min}}$ holds. Additionally, $S_{(X_q,Y_q)} \subset \overline{S_{\min}}$ because of the definition of $S_{(X_q,Y_q)}$ and $y \ge 0$. Therefore $\overline{S_{(X_q,Y_q)}} \subset \overline{S_{\min}}$ holds. In the case of $x \ge x_q$, we similarly prove $\overline{S_{(X_q,Y_q)}} \subset \overline{S_{\max}}$ because $x_{\max} < x_q$. Accordingly, $\overline{S_{(X_q,Y_q)}} \subset \overline{S_{\min} \cup S_{\max}}$ holds. This holds in the case of $X_q = X_{\min}$ or $X_q = X_{\max}$. Therefore, for all $(X, Y) \in \partial D$, this relationship holds, and the necessary condition of Proposition 1. is proved.

(ii) Proof of the sufficient condition of Proposition 1.
We assume that $g(X, Y) > 0$ holds in $(X, Y) \in \partial D$. By

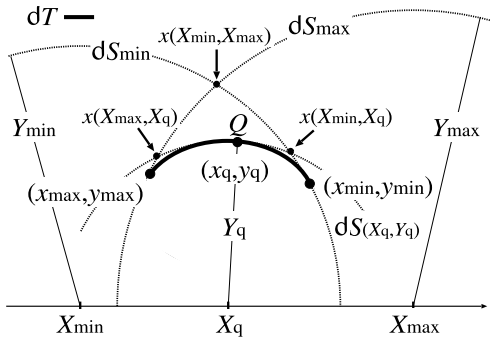


**Fig. A·3** Arrangement $Q$, $\partial S_{\min}$ and $\partial S_{\max}$ for the proof of the necessary condition of Proposition 1.

Eq. (6), $\partial T = \partial S_+$ holds. We define $P \in \partial T$ as $(x_p, y_p)$. In this region, $\overline{S_+} \subset \overline{S_{\max} \cup S_{\min}}$ holds. Moreover, $P \in \overline{S}_+$ holds because $\partial T = \partial S_+$ and $\partial S_+ \subset \overline{S}_+$ hold. Here $P = (x_p, y_p) \in \partial T$ should exist where $x_{\min} < x_p < x_{\max}$ holds. We define $(X_p, Y_p) \in \partial D$ which is transformed from $(x_p, y_p)$ with BST. With Prop. 2, $(x_p - X_{\min})^2 + y_p^2 > Y_{\min}^2$, and $(x_p - X_{\max})^2 + y_p^2 > Y_{\max}^2$ holds because $g(X, Y) > 0$ and $(x_p - X_p)^2 + y_p^2 = Y_p^2$ holds. Therefore $P \notin \overline{S}_+$ holds because $P \notin \overline{S_{\min}}$ and $P \notin \overline{S_{\max}}$. However this relationship contradicts the previous assumption. Therefore the sufficient condition of Proposition 1 is proved.

**Shouhei Kidera** received a B.E. degree from Kyoto University in 2003 and an M.E. degree from Graduate School of Informatics, Kyoto University in 2005. He is currently studying for a Ph.D. degree at Graduate School of Informatics, Kyoto University. His current research interest is in digital signal processing. He is a member of the IEEE.

**Takuya Sakamoto** was born in Nara, Japan in 1977. Dr. Sakamoto received his B.E. degree from Kyoto University in 2000, and his M.I. and Ph.D. degrees from Graduate School of Informatics, Kyoto University in 2002 and 2005, respectively. He is a research associate in the Department of Communications and Computer Engineering, Graduate School of Informatics, Kyoto University. His current research interest is in signal processing for UWB pulse radars. He is a member of the IEEJ and the IEEE.

**Toru Sato** received his B.E., M.E., and Ph.D. degrees in electrical engineering from Kyoto University, Kyoto, Japan in 1976, 1978, and 1982, respectively. He has been with Kyoto University since 1983 and is currently a Professor in the Department of Communications and Computer Engineering, Graduate School of Informatics. His major research interests have been system design and signal processing aspects of atmospheric radars, radar remote sensing of the atmosphere, observations of precipitation using radar and satellite signals, radar observation of space debris, and signal processing for subsurface radar signals. Dr. Sato was awarded Tanakadate Prize in 1986. He is a member of the Society of Geomagnetism and Earth, Planetary and Space Sciences, the Japan Society for Aeronautical and Space Sciences, the Institute of Electrical and Electronics Engineers, and the American Meteorological Society.